Hue University Journal of Science: Natural Science
Vol. 134, No. 1D, 23–31, 2025

pISSN 1859-1388
eISSN 2615-9678

Synthesis of Cu- and Ag-modified flower-like $Ni(OH)_2$ nanocomposites

Vu Hung Sinh[1], Nguyen Thi Cam Dieu[2], Nguyen Duong Thien[3], Huynh Thi Tuy Ngoc[2], Nguyen Dang Giang Chau[2], Nguyen Duc Cuong[1,3]*

[1] University of Education, Hue University, Hue, Vietnam
[2] University of Sciences, Hue University, Hue, Vietnam
[3] School of Hospitality and Tourism – Hue University, Hue, Vietnam

* Correspondence to Nguyen Duc Cuong <nguyenduccuong@hueuni.edu.vn>

(*Received: 11 December 2025; Revised: 14 December 2025; Accepted: 15 December 2025*)

Abstract. In this report, a simple template-free hydrothermal method was used to synthesise flower-like $Ni(OH)_2$ structures modified with Ag and Cu. The $Ni(OH)_2$ microflowers were formed via the self-assembly of ultrathin nanosheets with a thickness of approximately 2–3 nm. The incorporation of Ag and Cu at appropriate concentrations preserved the three-dimensional flower-like architecture of $Ni(OH)_2$. For the Ag-$Ni(OH)_2$ composite, Ag nanoparticles were uniformly dispersed on the $Ni(OH)_2$ nanosheets. In contrast, no $Cu(OH)_2$ phase was detected in the Cu-$Ni(OH)_2$ composite, likely because of Cu substituting the Ni sites within the $Ni(OH)_2$ lattice. Owing to their unique three-dimensional (3D) flower-like structure, large specific surface area, and enhanced physicochemical properties introduced by metal modification, these materials are potentially suitable for applications in electrochemical sensing, catalysis, and biomedical fields.

Keywords: nanocomposite, Cu-$Ni(OH)_2$, Ag-$Ni(OH)_2$, flower-like architecture

1 Introduction

Nanomaterials are materials with nanoscale (1–100 nm) dimensions or contain nanoscale structures within or on their surfaces. A nanometer corresponds approximately to five silicon atoms or ten hydrogen atoms aligned in a row [1]. Such an extremely small scale imparts nanomaterials with unique properties that are markedly different from those of bulk materials. Their ultrafine size results in a large specific surface area, thereby enhancing chemical and physical properties, including electrical conductivity, magnetism, optical characteristics, and catalytic activity. Accordingly, nanomaterials have attracted significant attention for diverse applications, such as biomedicine, information technology, environmental protection, and energy [2]. To date, their development has been guided by strategies that include multi-component material design [3], morphology control, surface functionalisation [4], and crystal defect engineering [5], yielding a variety of novel and intriguing properties.

Transition metal oxides, metal oxides, and hydroxides represent an important class of materials because of their intriguing properties, such as magnetic, optical, and electrical characteristics [6–8]. Among them, nickel hydroxide ($Ni(OH)_2$) has demonstrated significant potential in several key applications, such as biosensing, energy storage, and catalysis. $Ni(OH)_2$ is considered a promising biosensor material owing to its low toxicity, cost-effectiveness, high biocompatibility, and strong interactions with biomolecules [9]. Rahmati et al. [10] functionalised screen-printed carbon electrodes with a layer of $Ni(OH)_2$ nanoparticles, which enhanced interactions with the spike protein of SARS-CoV-

2. This biosensor exhibited high sensitivity and specificity, offering a highly effective immunodiagnostic approach for detecting SARS-CoV-2 antibodies. $Ni(OH)_2$ has also been explored as a promising electrode material for supercapacitors. It has been investigated as a pseudocapacitive material and remains a key component in electric vehicles and wearable electronics because of its unique structure, high theoretical capacitance, and low cost [11]. Li et al. [12] demonstrated that amorphous $Ni(OH)_2$ nanospheres exhibit excellent electrochemical performance, making them suitable as advanced electrode materials for pseudocapacitors with high specific capacitance, energy density, power density, and long cycle life. Wu et al. [13] reported that $Ni(OH)_2$ also shows considerable promise as an electrocatalyst for the urea oxidation reaction, applicable in energy conversion devices such as direct urea fuel cells.

Up to present, various $Ni(OH)_2$ nanostructures have been successfully synthesised with different methods, including nanorods [14], nanoparticles [15], hexagonal nanosheets [5], and flower-like architectures [16]. These diverse morphologies provide enhancements in the $Ni(OH)_2$ physicochemical properties and also serve as attractive precursors for the fabrication of NiO nanostructures.

In addition, doping or integrating $Ni(OH)_2$ with functional materials has emerged as an effective strategy to create advanced hybrid materials. Shakir et al. [17] demonstrated that a $Ni(OH)_2$-based nanohybrid incorporating 5% carbon nanotubes exhibits superior electrical conductivity and specific capacitance compared with pristine $Ni(OH)_2$, while also showing reduced charge-transfer resistance. Owing to these characteristics, the β-$Ni(OH)_2$@CNT hybrid is considered a highly promising material for positive electrode in next-generation energy storage devices. Xu et al. [18] suggested that the crystallinity, morphology, and electronic structure of $Ni(OH)_2/Ti_3C_2T_x$ electrodes can be tuned through electrochemical activation, leading to improved conductivity and enhanced redox activity. Bao et al. [19] further found that $Ag/Ni(OH)_2$ nanosheet composites exhibit excellent catalytic activity for the reduction of 4-nitrophenol by $NaBH_4$. In this hybrid, $Ni(OH)_2$ serves as a crucial supporting matrix for the formation of Ag nanoparticles, functioning not only as an efficient adsorbent for Ag^+ ions but also as a source of OH^- groups that accelerate the reaction. Therefore, the synthesis and modification of $Ni(OH)_2$ nanostructures with functional materials, particularly those containing semiconducting and noble metals with superior catalytic or electrochemical performance, represent an important and ongoing research direction.

In this study, we used a simple template-free hydrothermal method to successfully synthesise flower-like micro/nanostructured $Ni(OH)_2$. The three-dimensional structure of $Ni(OH)_2$, formed through the self-assembly of thin nanosheets, could be modified with functional components such as Ag and Cu. This modification can be conducted simultaneously during the synthesis of $Ni(OH)_2$ by adding an appropriate amount of Cu salt into the reaction solution, or it can be performed after the $Ni(OH)_2$ structure has been successfully synthesised by decorating Ag nanoparticles onto the nanosheet surfaces. While Cu atoms substitute Ni sites within the $Ni(OH)_2$ crystal lattice, the Ag–$Ni(OH)_2$ composite exhibits well-dispersed Ag nanoparticles anchored onto the $Ni(OH)_2$ nanosheets. Owing to their unique hierarchical 3D spherical structures, the intriguing physicochemical characteristics of $Ni(OH)_2$, and the incorporation of Ag and Cu nanoparticles, these composites exhibit great potential for

pISSN 1859-1388
eISSN 2615-9678

applications in biosensing, electrocatalysis, and biomedical materials.

2 Experimental

2.1 Materials

All the reagents were of analytical grade and used without further purification. $Ni(NO_3)_2{\cdot}6H_2O$, $AgNO_3$, and $Cu(NO_3)_2{\cdot}3H_2O$ were purchased from Sigma-Aldrich, and urea was purchased from Guangzhou, China.

2.2 Synthesis and characterisations

Synthesis of flower-like $Ni(OH)_2$ nano/microstructures

$Ni(OH)_2$ nano/microstructures were synthesised following our previous report [16] with minor modifications. First, 1.24 g of $Ni(NO_3)_2{\cdot}6H_2O$ and 13.5 g of urea were dissolved in 435 mL of water. The mixture was stirred for 15 min with a magnetic stirrer, transferred into a Teflon-lined autoclave, and hydrothermally treated at 60 °C for 12 h. It was then further treated at 90 °C for an additional 8 h. After the hydrothermal process, the autoclave was allowed to cool naturally to ambient temperature. The solid product was collected by centrifugation, washed with water and ethanol, and dried at 60 °C for 24 h to obtain the $Ni(OH)_2$ nanomaterial.

Synthesis of Ag-modified flower-like $Ni(OH)_2$ nanocomposite

An amount of 0.3 g of the as-synthesised $Ni(OH)_2$ was dispersed in 100 mL of water and stirred at 70 °C for 15 min. Subsequently, x mL of a 1% $AgNO_3$ solution (x = 0.5, 1, 2, 3 mL) was added, followed by the rapid addition of 2 mL of freshly prepared 2% $NaBH_4$. The mixture was maintained at 70 °C and stirred for 1 h, then cooled naturally to ambient temperature. It was subsequently centrifuged, washed with water and ethanol, and dried at 60 °C for 24 h to obtain Ag-modified $Ni(OH)_2$ nanocomposites. The resulting samples are denoted as xAg-$Ni(OH)_2$, where x represents the volume of the 1% $AgNO_3$ solution added.

Synthesis of Cu-modified flower-like $Ni(OH)_2$ nanocomposites

The synthesis procedure was identical to that of pure flower-like $Ni(OH)_2$ structures. A defined amount of $Cu(NO_3)_2{\cdot}3H_2O$ was added to the precursor mixture at an x% molar ratio relative to $Ni(NO_3)_2{\cdot}6H_2O$, where x = 1, 3, 5, and 7%. The resulting Cu-modified samples are denoted as x%Cu-$Ni(OH)_2$.

Material characterisation

The crystal phases of the samples were characterised by means of X-ray diffraction (XRD, Bruker D8 Advance) with Cu–Kα radiation (1.54056 Å). Scanning electron microscopy (SEM, JSM-5300LV) and energy-dispersive X-ray spectroscopy (EDX) were employed to analyse the morphology and elemental composition of the samples, respectively. Transmission electron microscopy (TEM) was performed with a JEOL JEM 1230 instrument. The specific surface area was determined via Brunauer–Emmett–Teller (BET) analysis based on nitrogen adsorption-desorption isotherms (Micromeritics Tristar 3030), while the pore size distribution of the nanomaterials was calculated with the Barrett–Joyner–Halenda (BJH) method.

3 Results and discussion

Fig. 1 presents the characteristic SEM, TEM, and XRD analysis results of the single-phase $Ni(OH)_2$ material. As shown in Fig. 1a, the material exhibits a flower-like spherical morphology with a porous, mesh-like surface. The higher-resolution SEM image reveals that the 3D spherical architecture is constructed from interwoven

nanosheets with a thickness of approximately 2–3 nm. In addition, the TEM image provides a more precise visualisation of the ultrathin $Ni(OH)_2$ nanosheets, where a low contrast arises from the insufficient sheet thickness to strongly scatter the electron beam, resulting in brighter regions in the TEM micrograph.

The XRD pattern exhibits diffraction peaks at $2\theta \approx 11.9$, 24.30, 33.25, and 59.44°, corresponding to the (003), (006), (101), and (110) crystal planes of α-$Ni(OH)_2$ (JCPDS No. 38-0715). No diffraction peaks associated with impurities or the β-$Ni(OH)_2$ phase are observed, confirming the high purity of the synthesised material.

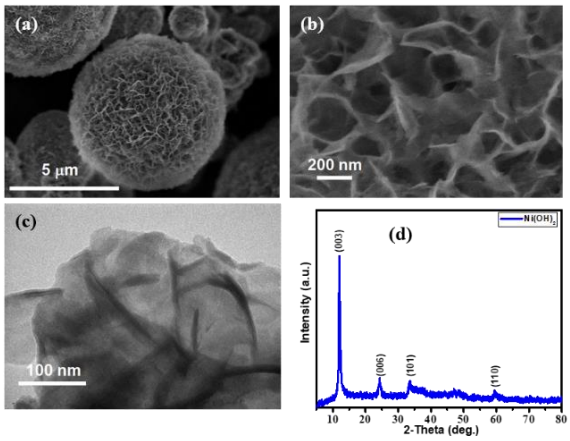

Fig. 1. SEM images (a, b); TEM image (c); XRD pattern (d) of the flower-like $Ni(OH)_2$ architecture

Fig. 2 shows the SEM images of flower-like $Ni(OH)_2$ materials modified with varying Cu contents ranging from 1 to 7%. The results indicate that Cu modification significantly changes the morphology compared with the pristine $Ni(OH)_2$. For the 1% Cu sample, the SEM images in Figs. 2a and 2b show that the flower-like structure similar to pristine $Ni(OH)_2$ is still maintained. When the Cu content increases to 3%, the flower-like morphology gradually collapses, as shown in Figs. 2c and 2d. For samples with higher Cu contents (5% Cu and 7% Cu, Figs. 2e–2h), the flower-like structure is completely disrupted, and the material forms interconnected nanosheets. This phenomenon can be attributed to the fact that the modification process often alters the crystal structure of the host material and introduces defects into the lattice [20].

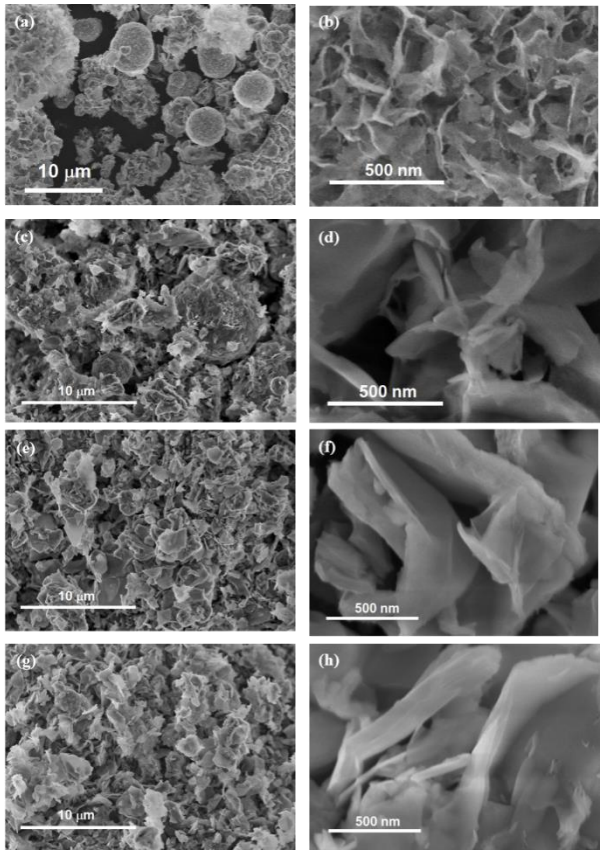

Fig. 2. SEM images of the 1%Cu-$Ni(OH)_2$ (a, b); 3%Cu-$Ni(OH)_2$ (c, d); 5%Cu-$Ni(OH)_2$ (e, f); 7%Cu-$Ni(OH)_2$ (g, h) samples

The phase composition of the Cu-doped $Ni(OH)_2$ materials was characterised by using XRD. The results are presented in Fig. 3. Fig. 3a shows that the $Ni(OH)_2$ samples doped with different Cu contents exhibit the characteristic peaks of single-phase $Ni(OH)_2$, with no peaks corresponding to Cu-related compounds. This may be attributed to the incorporation of Cu atoms into the $Ni(OH)_2$ lattice through isomorphic substitution. In addition, the intensity of diffraction peaks of $Ni(OH)_2$ gradually decreases

pISSN 1859-1388
eISSN 2615-9678

as the initial Cu doping content increases, indicating that the $Ni(OH)_2$ crystal lattice is significantly altered when Ni sites are substituted by Cu. The diffraction peak position of the (003) crystal plane for the 5%Cu-$Ni(OH)_2$ and 7%Cu-$Ni(OH)_2$ samples shows a slight shift toward higher angles, confirming that the doping process modifies the $Ni(OH)_2$ lattice structure, particularly at high Cu concentrations. This observation is consistent with the SEM results shown in Fig. 2.

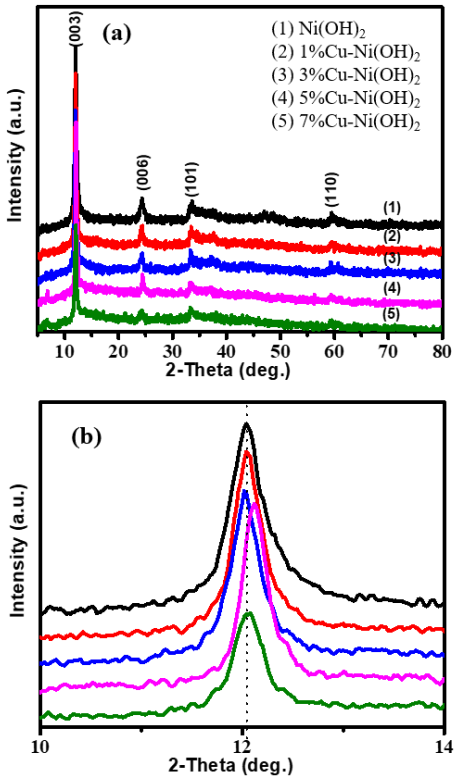

Fig. 3. (a) XRD patterns of $Ni(OH)_2$ and Cu-doped $Ni(OH)_2$ with different Cu contents; (b) XRD peak positions of the (003) crystal plane for the samples

The elemental composition of the $Ni(OH)_2$ and Cu-doped $Ni(OH)_2$ samples was characterised by means of EDX, and the results are presented in Fig. 4 and Table 1. As shown in Fig. 4a, the single-phase $Ni(OH)_2$ sample contains two elements, Ni and O, with an O/Ni ratio of approximately 2. In contrast, the Cu-doped $Ni(OH)_2$ nanomaterials contain three elements: Ni, O, and Cu. As the initial Cu content used for doping increases, the intensity of the Cu peak in the EDX digractogram becomes more pronounced. This result is consistent with the elemental contents presented in Table 1, which shows that the Cu content increases linearly from the 1%Cu-$Ni(OH)_2$ sample to the 7%Cu-$Ni(OH)_2$ sample. In addition, the atomic ratio of Ni/Cu is fairly consistent with the initial ratio of the precursor salts used.

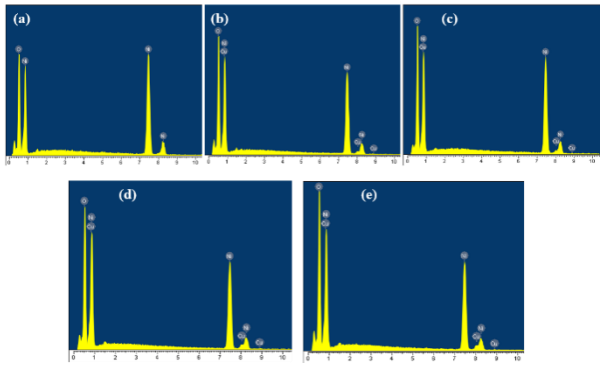

Fig. 4. EDX spectra of (a) $Ni(OH)_2$; (b) 1%Cu-$Ni(OH)_2$; (c) 3%Cu-$Ni(OH)_2$; (d) 5%Cu-$Ni(OH)_2$; (e) 7%Cu-$Ni(OH)_2$

The Ag-modified micro/nano spherical $Ni(OH)_2$ materials were also characterised by using SEM, TEM, XRD, and EDX. Fig. 5 shows the SEM images of the Ag-$Ni(OH)_2$ microspheres with different Ag contents (controlled by varying the amount of 1% $AgNO_3$ solution added during the synthesis). The results indicate that the original spherical structure of $Ni(OH)_2$ is well preserved despite changes in the Ag doping content. This may be attributed to the two-step synthesis process. In the first stage, the micro/nano spherical $Ni(OH)_2$ structure formed stably. In the second stage, Ag modification occurs only on the material surface, causing minimal impact on the crystal structure of $Ni(OH)_2$. Higher-resolution SEM images show the formation of Ag nanoparticles on the $Ni(OH)_2$ surface. As the initial Ag doping content increases, the number of Ag nanoparticles formed on the $Ni(OH)_2$ surface also increases.

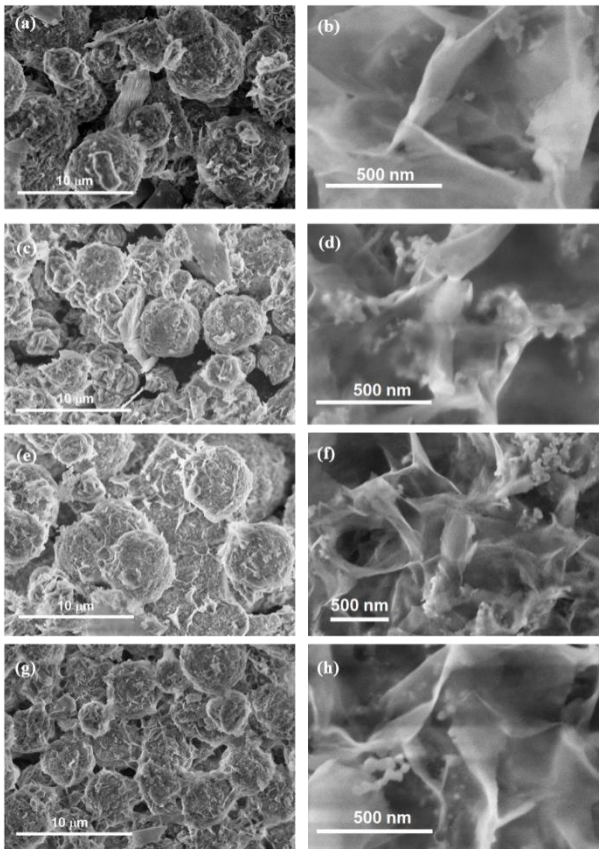

Fig. 5. SEM images of the 0.5Ag-Ni(OH)$_2$ (a, b); 1Ag-Ni(OH)$_2$ (c, d); 2Ag-Ni(OH)$_2$ (e, f); 3Ag-Ni(OH)$_2$ (g, h) samples

The XRD patterns of the Ag-modified Ni(OH)$_2$ materials shown in Fig. 6 reveal that, in addition to the characteristic peaks of Ni(OH)$_2$, a diffraction peak appears at approximately 2θ ~ 38.20°, corresponding to the (111) crystal plane of Ag. Notably, the intensity of this peak increases progressively with the initial Ag content, confirming the successful modification of Ag on the Ni(OH)$_2$ surface.

To further confirm the successful modification of Ag on the Ni(OH)$_2$ surface, the materials were additionally characterised by means of EDX, and the results are presented in Fig. 7 and Table 2. The results show that, in addition to Ni and O—the main elements of Ni(OH)$_2$—the element Ag also appears in all samples. The data in Table 2 indicate that the percentage of Ag in the samples increases correspondingly with the initial amount of Ag added. The combined XRD and EDX results demonstrate that Ag can be successfully incorporated onto the surface of Ni(OH)$_2$ at different concentrations.

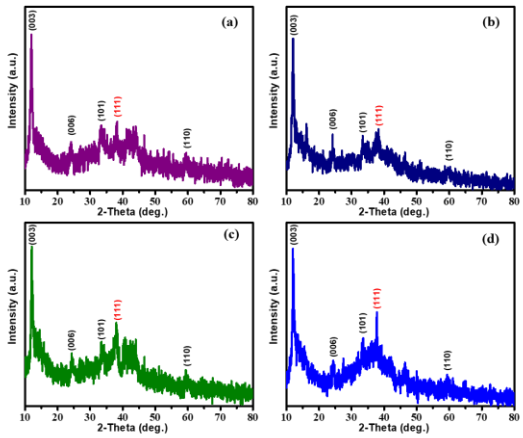

Fig. 6. XRD patterns of 0.5Ag-Ni(OH)$_2$ (a); 1Ag-Ni(OH)$_2$ (b); 2Ag-Ni(OH)$_2$ (c); 3Ag-Ni(OH)$_2$ (d)

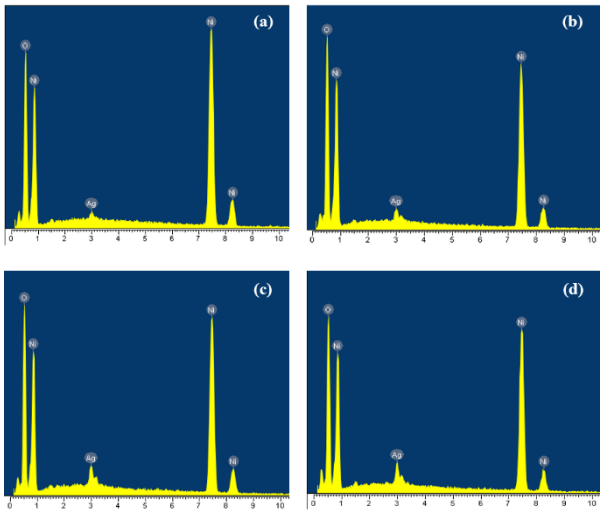

Fig. 7. EDX spectra of the 0.5Ag-Ni(OH)$_2$ (a); 1Ag-Ni(OH)$_2$ (b); 2Ag-Ni(OH)$_2$ (c); 3Ag-Ni(OH)$_2$ (d) samples

pISSN 1859-1388
eISSN 2615-9678

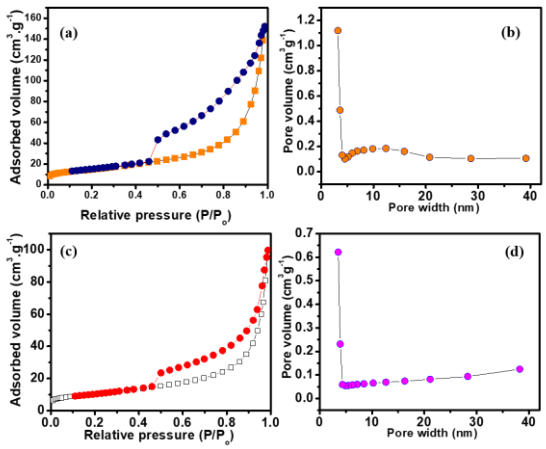

Fig. 8. N2 adsorption/desorption isotherms and corresponding BJH pore size distribution curves of the 3%Cu-Ni(OH)2 (a, b); 1Ag-Ni(OH)2 (c, d) materials

To determine the porous structure of the materials, we analysed the N_2 adsorption/desorption isotherms of the 3%Cu-Ni(OH)2 and 1Ag-Ni(OH)2 samples (representative samples with intermediate doping levels that still maintain a well-defined 3D spherical structure), as shown in Fig. 8. The results reveal that both materials exhibit type IV isotherms according to IUPAC classification, with H3 hysteresis loops, characteristic of mesoporous materials. The 3%Cu-Ni(OH)2 and 1Ag-Ni(OH)2 samples exhibit a large specific surface area of 53 m^2/g and 37 m^2/g, respectively. The formation of Ag nanoparticles on the Ni(OH)2 surface may partially block the pore system of the 3D spherical structure, resulting in a smaller specific surface area for 1Ag-Ni(OH)2 compared with 3%Cu-Ni(OH)2.

The pore size distribution curves of the two materials are also quite similar, with pore systems falling within the mesoporous range. These functional materials possess larger specific surface areas than the micro-flower Ni(OH)2 structure previously reported by us [16], and other Ni(OH)2 nanostructures such as hexagonal nanosheets [21], nanocones, and nanoflowers [22]. In addition, with their mesoporous networks, these materials show great potential for applications in catalysis, adsorption, sensing, and biomedicine.

Table 1. Elemental composition of Ni(OH)2 and Cu-doped Ni(OH)2 with different doping levels

Element	Sample									
	Ni(OH)2		1%Cu-Ni(OH)2		3%Cu-Ni(OH)2		5%Cu-Ni(OH)2		7%Cu-Ni(OH)2	
	Wt. (%)	At. (%)	Wt. (%)	At. (%)	Wt. (%)	At. (%)	Wt. (%)	At. (%)	Wt. (%)	At. (%)
O	35.19	66.58	38.16	69.38	39.09	70.23	40.03	71.08	41.81	72.59
Ni	64.81	33.42	61.12	30.29	59.06	28.93	57.18	27.68	54.43	25.76
Cu	0	0	0.72	0.33	1.85	0.84	2.79	1.24	3.76	1.65

Table 2. Elemental composition of Ag-modified Ni(OH)2 with different Ag contents

Element	Sample							
	0.5Ag-Ni(OH)2		1Ag-Ni(OH)2		2Ag-Ni(OH)2		3Ag-Ni(OH)2	
	Wt. (%)	At. (%)	Wt. (%)	At. (%)	Wt. (%)	At. (%)	Wt. (%)	At. (%)
O	31.4	62.87	37.77	69.46	35.85	67.86	36.25	68.3
Ni	67.36	36.76	59.39	29.76	60.12	31.01	59.3	30.45
Ag	1.24	0.37	2.85	0.78	4.04	1.13	4.45	1.24

4 Conclusions

In this report, we successfully synthesised two functional nanocomposite materials, Cu-$Ni(OH)_2$ and Ag-$Ni(OH)_2$. The materials exhibit a unique spherical architecture constructed primarily from nanosheets. Characteristic results reveal that Cu substitutes Ni through isomorphic substitution within the $Ni(OH)_2$ crystal lattice, whereas Ag nanoparticles are dispersed on the surface of $Ni(OH)_2$. With low Cu doping levels (1% and 3%), the 3D spherical structure of $Ni(OH)_2$ is preserved. Meanwhile, Ag is introduced onto a pre-formed and stable 3D $Ni(OH)_2$ structure; therefore, even with varying Ag contents, the spherical morphology of $Ni(OH)_2$ remains well maintained.

With their unique physicochemical properties and large specific surface areas, the Cu-$Ni(OH)_2$ and Ag-$Ni(OH)_2$ nanocomposites exhibit great potential for various applications such as catalysis, biosensing, and biomedical fields.

Acknowledgement

We are grateful to Hue University for funding our research under grant number DHH2024-10-39.

References

1. Mordorski B, Landriscina A, Friedman A. Chapter 3 - An Overview of Nanomaterials in Dermatology. In: Hamblin MR, Avci P, Prow TW, editors. Nanoscience in Dermatology. Boston: Academic Press; 2016. p. 31-46.
2. Baig N, Kammakakam I, Falath W. Nanomaterials: a review of synthesis methods, properties, recent progress, and challenges. Materials Advances. 2021;2(6):1821-71.
3. Cuong ND, Sinh VH, Quang DT, Hoa LT, Tan VV, Mai HD, et al. 3D porous p-n α-Fe_2O_3/NiO heteronanostructure for ultrasensitive H_2S gas sensor. Current Applied Physics. 2024;59:153-64.
4. Hoa LT, Cuong ND, Hoa TT, Khieu DQ, Long HT, Quang DT, et al. Synthesis, characterization, and comparative gas sensing properties of tin dioxide nanoflowers and porous nanospheres. Ceramics International. 2015;41(10, Part B):14819-25.
5. Dang TK, Cuong ND, Sinh VH, Long HT, Hieu LT, Thy PNA, et al. Hexagonal annular-NiO nanoarchitecture with local p-n homojunctions: Novel formation mechanism and H2S gas sensing properties. Journal of Alloys and Compounds. 2023;933:167782.
6. Harish Kumar K, Ananda HT, Ravishankar DK, Madhu H, Thirumala S. A review on nano metal oxides and their nanocomposites for photocatalytic degradation of dyes. Sustainable Chemistry One World. 2025;6:100055.
7. Safarpour M, Arefi-Oskoui S, Khataee A. A review on two-dimensional metal oxide and metal hydroxide nanosheets for modification of polymeric membranes. Journal of Industrial and Engineering Chemistry. 2020;82:31-41.
8. Cuong ND, Quang DT. Quang, Progress through synergistic effects of heterojunction in nanocatalysts – Review. Vietnam J Chem. 2020;58(4):434-63.
9. Ko C-Y, Huang J-H, Raina S, Kang WP. A high performance non-enzymatic glucose sensor based on nickel hydroxide modified nitrogen-incorporated nanodiamonds. Analyst. 2013;138(11):3201-8.
10. Rahmati Z, Roushani M, Hosseini H, Choobin H. An electrochemical immunosensor using SARS-CoV-2 spike protein-nickel hydroxide nanoparticles bio-conjugate modified SPCE for ultrasensitive detection of SARS-CoV-2 antibodies. Microchemical Journal. 2021;170:106718.
11. Nie Y, Pan J, Jiang W, Pan J, Liu J, Sun Y, et al. A facile preparation of Nickel Foam-supported $Ni(OH)_2$ nano arrays via in-situ etching method with superior bendable electrochemical performance for wearable power supply. Journal of Alloys and Compounds. 2020;835:155293.
12. Li HB, Yu MH, Wang FX, Liu P, Liang Y, Xiao J, et al. Amorphous nickel hydroxide nanospheres with ultrahigh capacitance and energy density as electrochemical pseudocapacitor materials, Nature Communications. 2013;4(1):1894.
13. Wu T-H, Hou B-W. Superior catalytic activity of α-$Ni(OH)_2$ for urea electrolysis. Catalysis Science & Technology. 2021;11(12):4294-300.

pISSN 1859-1388
eISSN 2615-9678

14. Wei W, Chen W, Mi L, Xu J, Zhang J. High-rate performance aqueous-based supercapacitors at −30 °C driven by novel 1D $Ni(OH)_2$ nanorods and a two-solute electrolyte. Journal of Materials Chemistry A. 2021;9(42):23860-72.

15. Wang R, Lang J, Liu Y, Lin Z, Yan X. Ultra-small, size-controlled Ni(OH)2 nanoparticles: elucidating the relationship between particle size and electrochemical performance for advanced energy storage devices. NPG Asia Materials. 2015;7(6):e183-e.

16. Trung DD, Cuong ND, Quang PL, Ngoc Anh NT, Quang DT, Nam PC, et al. Facile post-synthesis and gas sensing properties of highly porous NiO microspheres. Sensors and Actuators A: Physical. 2019;296:110-20.

17. Shakir I, Almutairi Z, Shar SS, Nafady A. Nickel hydroxide nanoparticles and their hybrids with carbon nanotubes for electrochemical energy storage applications. Results in Physics. 2020;17:103117.

18. Xu C, Dai L, Zhao Y, Li S, Wu Y, Wu X, et al. Electrochemical Activation-Induced Structural Transformation in $Ni(OH)_2/Ti_3C_2T_x$/NF Systems with Enhanced Electrochemical Performance for Hybrid Supercapaci. Energy Environ Mater. 2024;7(4):e12672.

19. Bao F, Tan F, Wang W, Qiao X, Chen J. Facile preparation of $Ag/Ni(OH)_2$ composites with enhanced catalytic activity for reduction of 4-nitrophenol. RSC Advances. 2017;7(23):14283-9.

20. Freire EBV, Santos ALdS, Bispo GFdC, Macedo ZS, Jackson RA, Valerio MEG. Local modification of the crystalline structure due to co-doping with RE3+ in cadmium metasilicate. Ceramics International. 2024;50(13, Part A):22534-43.

21. Zhou T, Qiu Z, Hao C, Gao Q, Zhao Y, Zhao J, et al. Enhanced asymmetric supercapacitor performance of NiOOH electrodes from hexagonal $Ni(OH)_2$ nanosheets via low-concentration OH^--mediated growth and galvanostatic oxidation. Journal of Energy Storage. 2025;137:118558.

22. Yan Y, Cheng G, Wang P, He D, Chen R. Facile hydrothermal selective fabrication of $Ni(OH)_2$ and $Ni(HCO_3)_2$ nanoparticulates and their electrochemical performances. RSC Advances. 2014;4(90):49303-7.